

Comparative study of correlation effects in CaVO_3 and SrVO_3

I.A. Nekrasov,^{1,2} G. Keller,² D.E. Kondakov,^{1,2,3} A.V. Kozhevnikov,^{1,2,3}

Th. Pruschke*,² K. Held,⁴ D. Vollhardt,² and V.I. Anisimov^{1,2}

¹*Institute of Metal Physics, Russian Academy of Sciences-Ural Division,
620219 Yekaterinburg GSP-170, Russia*

²*Theoretical Physics III, Center for Electronic Correlations and Magnetism,
University of Augsburg, 86135 Augsburg, Germany*

³*Department of Theoretical Physics and Applied Mathematics,
USTU, 620002 Yekaterinburg Mira 19, Russia*

⁴*Max Planck Institute for Solid State Research,
Heisenbergstr. 1, 70569 Stuttgart, Germany*

Abstract

We present parameter-free LDA+DMFT (local density approximation + dynamical mean field theory) results for the many-body spectra of cubic SrVO_3 and orthorhombic CaVO_3 . Both systems are found to be strongly correlated metals, but *not* on the verge of a metal-insulator transition. In spite of the considerably smaller V-O-V bond angle in CaVO_3 the LDA+DMFT spectra of the two systems for energies $E < E_F$ are very similar, their quasiparticle parts being almost identical. The calculated spectrum for $E > E_F$ shows more pronounced, albeit still small, differences. This is in contrast to earlier theoretical and experimental conclusions, but in good agreement with recent bulk-sensitive photoemission and x-ray absorption experiments.

PACS numbers: 71.27.+a, 71.30.+h

I. INTRODUCTION

Transition metal oxides are an ideal laboratory for the study of electronic correlations in solids. In these materials, the $3d$ bands are comparatively narrow with width $W \approx 2-3$ eV so that electronic correlations, induced by the local Coulomb interaction $\bar{U} \approx 3-5$ eV, are strong. For $\bar{U}/W \ll 1$, we have a weakly correlated metal and the local density approximation (LDA) (see [1] for a review) works. In the opposite limit $\bar{U}/W \gg 1$ and for an integer number of $3d$ electrons, we have a Mott insulator with two separate Hubbard bands as described by Hubbard's I and III approximations [2] or the LDA+U method [3]. Transition metals are, however, in the "in-between" regime, $\bar{U}/W = \mathcal{O}(1)$, where the metallic phase is strongly correlated with coexisting *quasiparticle* peak at the Fermi level and Hubbard side bands.

Dynamical mean-field theory (DMFT) [4, 5, 6, 7, 8], a modern, non-perturbative many-body approach, is able to capture the physics in the whole range of parameters from $\bar{U}/W \ll 1$ to $\bar{U}/W \gg 1$ for model Hamiltonians, like the one-band Hubbard model (for an introduction into DMFT and its applications see [8]). And, with the recent merger [9, 10, 11] of LDA and DMFT, we are now able to handle this kind of correlation physics within realistic calculations for transition metal oxides.

A particularly simple transition metal oxide system is $\text{Ca}_{1-x}\text{Sr}_x\text{VO}_3$ with a $3d^1$ electronic configuration and a cubic perovskite lattice structure, which is ideal for SrVO_3 and orthorhombically distorted upon increasing the Ca-doping x . Fujimori *et al.* [12] initiated the present interest in this $3d^1$ series, reporting a pronounced lower Hubbard band in the photoemission spectra (PES) which cannot be explained by conventional LDA. Subsequently, thermodynamic properties were studied, and the Sommerfeld coefficient, resistivity, and paramagnetic susceptibility were found to be essentially independent of x [13].

On the other hand, PES [14], seemed to imply dramatic differences between CaVO_3 and SrVO_3 , with CaVO_3 having (almost) no spectral weight at the Fermi energy. Rozenberg *et al.* [15] interpreted these results in terms of the (DMFT) Mott-Hubbard transition in the half-filled single-band Hubbard model. With the same theoretical ansatz, albeit different parameters, the optical conductivity [16] and the PES experiments [17] for different dopings x were reproduced.

The puzzling discrepancy between these spectroscopic and the thermodynamic measure-

ments, suggesting a Mott-Hubbard metal-insulator transition or not, were resolved recently by bulk-sensitive PES obtained by Maiti *et al.* [17] and Sekiyama *et al.* [18, 19]. In the latter work it was shown that (i) the technique of preparing the sample surface (which should preferably be done by fracturing) is very important, and that (ii) the energy of the X-ray beam should be large enough to increase the photoelectron escape depth to achieve bulk-sensitivity. Theoretically, pronounced differences between SrVO₃ surface and bulk spectra were reported by Liebsch [20]. Besides bulk-sensitivity, the beam should provide a high instrumental resolution (about 100 meV in [18, 19]). With these experimental improvements, the PES of SrVO₃ and CaVO₃ were found to be almost identical [17, 18, 19], implying consistency of spectroscopic and thermodynamic results at last. This is also in accord with earlier 1s x-ray absorption spectra (XAS) by Inoue *et al.* [21] which differ only slightly above the Fermi energy, as well as with BIS data [14]. Parameterfree LDA+DMFT results by us [22], reported in the joint experimental and theoretical Letter by Sekiyama *et al.* [19], showed good agreement with the high-resolution bulk-sensitive PES. Independent LDA+DMFT calculations for 3d¹ vanadates, including SrVO₃ and CaVO₃ have been reported by Pavarini *et al.* [23]. Most recently Anisimov *et al.* employed a full-orbital computational scheme based on Wannier functions formalism for LDA+DMFT to calculate *total* densities of states for SrVO₃ which are in good agreement with new PES data. [24]

In this paper we present details of our LDA+DMFT calculation [22] which could not be included in the joint Letter [19]. In particular, we discuss the crystal structure of SrVO₃ and CaVO₃, explain the origin of the surprisingly small change in bandwidth of these two systems, and compare the calculated spectrum for energies $E > E_F$ with XAS data [21]. We start with discussing the structural differences between SrVO₃ and CaVO₃ in Section II A, based on the most recent crystallographic data provided by Inoue [26]. How these differences reflect in the LDA results is shown in Section II B, before we turn to the LDA+DMFT scheme in Sections III A and the effects of electronic correlations in Section III B. Section IV concludes our presentation.

II. SrVO_3 VS. CaVO_3 : STRUCTURAL DIFFERENCES AND LDA RESULTS

A. Structural differences

Both SrVO_3 and CaVO_3 are perovskites, with SrVO_3 in the ideal cubic structure $\text{Pm}\bar{3}\text{m}$ [27] (Fig. 1) and CaVO_3 in the orthorhombically distorted (GdFeO_3) Pbnm structure [26, 28] (Fig. 2). The ideal cubic structure of SrVO_3 implies that the VO_6 octahedra, the main structural elements of the crystal, are not distorted: The $\text{V-O}_{\text{basal}}$ and V-O_{apex} distances are the same, the $\text{O}_{\text{apex}}\text{-V-O}_{\text{basal}}$ and $\text{O}_{\text{basal}}\text{-V-O}_{\text{basal}}$ angles are 90° , and the V-O-V bond angles are exactly 180° . The substitution of the large Sr^{2+} ions by smaller Ca^{2+} ions leads to a tilting, rotation, and distortion of the VO_6 octahedra. Nonetheless, in CaVO_3 , both the $\text{V-O}_{\text{basal}}$ and the V-O_{apex} distances are practically the same. Therefore, the most important feature of the distortion is the change of the $\text{V-O}_{\text{basal}}\text{-V}$ and $\text{V-O}_{\text{apex}}\text{-V}$ angles, which determines the strength of the effective $\text{V}3d\text{-V}3d$ hybridization and, hence, the bandwidth. Due to the rotation and tilting of the octahedra both angles (one of them is marked as $\angle 123$ in Figs. 1 and 2) have the same value $\theta = 180^\circ$ for SrVO_3 and $\theta_{\text{basal}} \approx 161^\circ$, $\theta_{\text{plane}} \approx 163^\circ$ for CaVO_3 .

B. LDA results

The valence states of SrVO_3 and CaVO_3 consist of completely occupied oxygen $2p$ bands and partially occupied V $3d$ bands. Since the V ion has a formal oxidation of $4+$, there is one electron per V ion occupying the d -states (configuration d^1). In Figs. 3 and 4 the LDA density of states (DOS) are presented for both compounds, as calculated by the linearized muffin-tin orbitals method (LMTO) [29] with an orthogonal basis set of $\text{Sr}(5s, 5p, 4d, 4f)$, $\text{Ca}(4s, 4p, 3d)$, $\text{V}(4s, 4p, 3d)$, and $\text{O}(3s, 2p, 3d)$ orbitals [30]. These results are in agreement with previous LDA calculations in the basis of augmented plane waves (APW) by Tagekahara [31]. For a combination of the LDA band structure with many-body techniques [9] however, the atomic-like LMTO wave functions employed here are particularly convenient. As is apparent from Figs. 3 and 4, the $\text{O-}2p$ states lie between -7.5eV and -2.0eV in SrVO_3 and between -6.5eV and -1.5eV in CaVO_3 . The $3d$ states of V are located between -1.1eV and 6.5eV in SrVO_3 and between -1.0eV and 6.5eV in CaVO_3 . These results are in agreement with previous LDA calculations in the basis of augmented plane waves (APW) by Tagekahara

[31], but for our purposes LMTO is more appropriate.

In both compounds, the V ions are in a octahedral coordination of oxygen ions. The octahedral crystal field splits the V-3d states into three t_{2g} orbitals and two e_g orbitals. In the cubic symmetry of SrVO₃, hybridization between t_{2g} and e_g states is forbidden, and the orbitals within both subbands are degenerate. In contrast, the distorted orthorhombic structure of CaVO₃ allows them to mix and the degeneracy is lifted. In the lower part of Figs. 3 and 4, we present these t_{2g} and e_g subbands of the V-3d band. For both Sr and Ca compounds, the reader can see an admixture of these Vanadium t_{2g} and e_g states to the oxygen 2p states in the energy region [-8 eV,-2 eV]. This is due to hybridization and amounts to 12% and 15% of the total t_{2g} weight for SrVO₃ and CaVO₃, respectively. The main t_{2g} (e_g) weight lies in the energy region [-1.1 eV,1.5 eV] ([0.0 eV,6.5 eV]) in SrVO₃ and [-1.0 eV,1.5 eV] ([0.2 eV,6.5 eV]) in CaVO₃. Since the energy difference between the centers of gravities of the t_{2g} and e_g subbands is comparable with the bandwidth, t_{2g} and e_g states can be considered as sufficiently separated in both compounds.

Let us now concentrate on the t_{2g} orbitals crossing the Fermi energy and compare the LDA t_{2g} DOS of SrVO₃ and CaVO₃. Most importantly, the one-electron t_{2g} LDA bandwidth of CaVO₃, defined as the energy interval where the t_{2g} DOS in Figs. 3 and 4 is non-zero, is found to be only 4% smaller than that of SrVO₃ ($W_{\text{CaVO}_3} = 2.5$ eV, $W_{\text{SrVO}_3} = 2.6$ eV); in general agreement with other LDA calculations [23]. This is in contrast to the expectation that the strong lattice distortion with a decrease of the V-O-V bond angle from 180° to 162° affects the t_{2g} bandwidth much more strongly. Such a larger effect indeed occurs in the e_g bands for which the bandwidth is reduced by 10%. To physically understand the smallness of the narrowing of the t_{2g} bands we have investigated a larger Hamiltonian consisting of e_g , t_{2g} , and oxygen p orbitals. We calculated the overall direct $d-d$ and the indirect $d-p-d$ hopping for this larger Hamiltonian. The predominant contribution to the e_g - e_g hopping is through a $d-p-d$ hybridization, which is considerably decreasing with the lattice distortion. This is also the case for the t_{2g} orbitals. However, for the t_{2g} orbitals, the direct $d-d$ hybridization is also important. This hybridization *increases* with the distortion since the t_{2g} orbital lobes point more directly towards each other in the distorted structure. Hopping parameters for individual orbitals change rather substantially from SrVO₃ to CaVO₃. But, altogether, a decreasing $d-p-d$ hybridization and an increasing $d-d$ hybridization results in a very small change of the t_{2g} bandwidth.

III. CORRELATION EFFECTS IN SrVO₃ AND CaVO₃

A. Dynamical Mean-Field Theory

As is well-known, LDA does not treat the effects of strong local Coulomb correlations adequately. To overcome this drawback, we use LDA+DMFT as a non-perturbative approach to study strongly correlated systems [9, 10, 11]. It combines the strength of the LDA in describing weakly correlated electrons in the s - and p -orbitals, with the DMFT treatment of the dynamics due to local Coulomb interactions. In the present paper we will discuss the relevant parts of the LDA+DMFT approach only briefly, referring the reader to Ref. [10, 11] for details.

The LDA+DMFT Hamiltonian can be written as

$$\hat{H} = \hat{H}_{\text{LDA}}^0 + U \sum_m \sum_i \hat{n}_{im\uparrow} \hat{n}_{im\downarrow} + \sum_{i m \neq m' \sigma \sigma'} (U' - \delta_{\sigma\sigma'} J) \hat{n}_{im\sigma} \hat{n}_{im'\sigma'}. \quad (1)$$

Here, the index i enumerates the V sites, m the individual t_{2g} orbitals and σ the spin. H_{LDA}^0 is the one-particle Hamiltonian generated from the LDA band structure with an averaged Coulomb interaction subtracted to account for double counting [9]; U and U' denote the local intra-orbital and inter-orbital Coulomb repulsions, and J is the exchange interaction.

We calculated these interaction strengths by means of the constrained LDA method [32] for SrVO₃, allowing the e_g states to participate in screening [33]. The resulting value of the averaged Coulomb interaction is $\bar{U} = 3.55$ eV ($\bar{U} = U'$ for t_{2g} orbitals [10, 34]) and $J = 1.0$ eV. The intra-orbital Coulomb repulsion U is then fixed by rotational invariance to $U = U' + 2J = 5.55$ eV. We did not calculate \bar{U} for CaVO₃ because the standard procedure to calculate the Coulomb interaction parameter between two t_{2g} electrons, screened by e_g states, is not applicable for the distorted crystal structure where the e_g and t_{2g} orbitals are not separated by symmetry. On the other hand, it is well-known that the change of the *local* Coulomb interaction is typically much smaller than the change in the DOS, which was found to depend only very weakly on the bond angle. That means that \bar{U} for CaVO₃ should be nearly the same as for SrVO₃. Therefore we used $\bar{U} = 3.55$ eV and $J = 1.0$ eV for both SrVO₃ and CaVO₃. This is also in agreement with previous calculations of vanadium systems [33] and experiments [16].

DMFT maps the lattice problem Eq. (1) onto a self-consistent auxiliary impurity problem, which is here solved numerically by the quantum Monte-Carlo (QMC) technique [35].

Combined with the maximum entropy method [36], this technique allows us to calculate spectral functions [37, 38, 39, 40].

A computationally important simplification is due to the fact that, in ideal cubic perovskites, the (degenerate) t_{2g} states do not mix with the (degenerate) e_g states. In this particular case, the self-energy matrix $\Sigma(z)$ is diagonal with respect to the orbital indices. Under this condition, the Green functions $G_m(z)$ of the lattice problem can be expressed in the DMFT self-consistency equation by the Hilbert transform of the non-interacting DOS $N_m^{(0)}(\omega)$:

$$G_m(z) = \int d\epsilon \frac{N_m^{(0)}(\epsilon)}{z - \Sigma_m(z) - \epsilon} . \quad (2)$$

This procedure avoids the rather cumbersome and problematic k -integration over the Brillouin zone by the analytical tetrahedron method [41]. We obtain $N_m^{(0)}(\epsilon)$ for SrVO₃ and CaVO₃ from the t_{2g} -projected DOS of Figs. 3 and 4 by truncating the contribution in the oxygen range below -1.5 eV and multiplying by a renormalization factor (to have maximally one electron per site and orbital). This procedure is employed as it resembles the three *effective* bands of t_{2g} character which cross the Fermi energy and are, hence, responsible for the low-energy physics.

B. LDA+DMFT(QMC) results and discussion

The calculated LDA+DMFT(QMC) spectra for SrVO₃ (right panel) and CaVO₃ (left panel) are presented in Fig. 5 for different temperatures. Due to genuine correlation effects, a lower Hubbard band at about -1.5 eV and an upper Hubbard band at about 2.5 eV is formed, with a well pronounced quasiparticle peak at the Fermi energy. The 4% difference in the LDA bandwidth between SrVO₃ and CaVO₃ is only reflected in some additional transfer of spectral weight from the quasiparticle peak to the Hubbard bands, and minor differences in the positions of the Hubbard bands. Clearly, the two systems are not on the verge of a Mott-Hubbard metal-insulator transition. Both, SrVO₃ and CaVO₃, are strongly correlated metals, though SrVO₃ is slightly less correlated than CaVO₃ with somewhat more quasiparticle weight, in accord with their different LDA bandwidth. As one can see from Fig. 5, the effect of temperature on the spectrum is small for $T \lesssim 700$ K.

In the left panel of Fig. 6, we compare our LDA+DMFT spectra (300K), which were multiplied with the Fermi function at the experimental temperature (20 K) and Gauss broadened

with the experimental resolution of 0.1 eV [18] with the experimental PES data obtained by subtracting the experimentally estimated surface and oxygen contributions. Due to the high photon energy (several hundred eV) [18], the PES transition matrix elements will have *no* strong energy dependence in the energy interval of a few eV studied here, which justifies that we do not take such matrix elements into account.

The quasiparticle peaks in theory and experiment are seen to be in very good agreement. In particular, their heights and widths are almost identical for both SrVO₃ and CaVO₃. The difference in the positions of the lower Hubbard bands may be partly due to (i) the subtraction of the (estimated) oxygen contribution which might also remove some *3d* spectral weight below -2 eV, and (ii) uncertainties in the *ab-initio* calculation of \bar{U} .

Since inverse photoemission spectroscopy (IPES) data for SrVO₃ and CaVO₃ are not yet available we compare [44] the calculated spectrum for energies $E > E_F$ with XAS data by Inoue *et al.* [21] (right panel of Fig. 6). We consider core-hole life time effects by Lorentz broadening the spectrum with 0.2 eV [42], multiply with the inverse Fermi function (80K), and apply Gauss broadening given by the experimental resolution of 0.36 eV [26]. Again, the overall agreement of the weights and positions of the quasiparticle and upper *t_{2g}* Hubbard band is good, including the tendencies when going from SrVO₃ to CaVO₃. For CaVO₃ (Ca_{0.9}Sr_{0.1}VO₃ in the experiment), the LDA+DMFT quasiparticle weight is somewhat lower than in experiment.

In contrast to one-band Hubbard model calculations, our material specific results reproduce the strong asymmetry around the Fermi energy w.r.t. weights and bandwidths. Our results also give a different interpretation of the XAS than in [21] where the maximum at about 2.5 eV was attributed solely to the *e_g* band. We find that also the *t_{2g}* upper Hubbard band contributes in this energy range.

The slight differences in the quasiparticle peaks (see Fig. 5) lead to different effective masses, namely $m^*/m_0 = 2.1$ for SrVO₃ and $m^*/m_0 = 2.4$ for CaVO₃. These theoretical values agree with $m^*/m_0 = 2 - 3$ for SrVO₃ and CaVO₃ as obtained from de Haas-van Alphen experiments and thermodynamics [13, 43]. We note that the effective mass of CaVO₃ obtained from optical experiments is somewhat larger, i.e., $m^*/m_0 = 3.9$ [16].

IV. CONCLUSION

In summary, we investigated the spectral properties of the correlated $3d^1$ systems SrVO_3 and CaVO_3 within the LDA+DMFT(QMC) approach. Constrained LDA was used to determine the average Coulomb interaction as $\bar{U} = 3.55$ eV and the exchange coupling as $J = 1.0$ eV. With this input we calculated the spectra of the two systems in a parameter-free way. Both systems are found to be strongly correlated metals, with a transfer of the majority of the spectral weight from the quasiparticle peak to the incoherent upper and lower Hubbard bands. The calculated DMFT spectra of SrVO_3 and CaVO_3 , and in particular the quasiparticle parts, are found to be very similar, differences being slightly more pronounced at energies above the Fermi energy. Our calculated spectra agree very well with recent bulk-sensitive high-resolution PES [18] and XAS [21] data, i.e., with the experimental spectrum below *and* above the Fermi energy. Both compounds are similarly strongly correlated metals; CaVO_3 is not on the verge of a Mott-Hubbard transition.

Our results are in contrast to previous theories and the expectation that the strong lattice distortion leads to a strong narrowing of the CaVO_3 bandwidth and, hence, to much stronger correlation effects in CaVO_3 . While the e_g bands indeed narrow considerably, the competition between decreasing $d-p-d$ and increasing $d-d$ hybridization leads to a rather insignificant narrowing of the t_{2g} bands at the Fermi energy. This explains why the k -integrated spectral functions of CaVO_3 and SrVO_3 are so similar. With our theoretical results confirming the new PES and XAS experiments, we conclude that the insulating-like behavior observed in earlier PES and BIS experiments on CaVO_3 must be attributed to surface effects [20].

V. ACKNOWLEDGMENTS

This work was supported by Russian Basic Research Foundation grant RFFI-GFEN-03-02-39024_a (VA,IN,DK), RFFI-04-02-16096 (VA,IN,DK) and the Deutsche Forschungsgemeinschaft through Sonderforschungsbereich 484 (DV,GK,IN) and in part by the joint UrO-SO project N22 (VA,IN), the Emmy-Noether program (KH), by Grant of President of Russian Federation for young scientists MK-95.2003.02 (IN), Dynasty Foundation and International Center for Fundamental Physics in Moscow program for young scientists 2004

(IN), Russian Science Support Foundation program for young PhD of Russian Academy of Science 2004 (IN).

*New permanent address: Institut für Theoretische Physik, Universität Göttingen, Friedrich-Hund-Platz 1, D-37077 Göttingen, Germany.

-
- [1] R. O. Jones and O. Gunnarsson, *Rev. Mod. Phys.* **61**, 689 (1989).
 - [2] J. Hubbard, *Proc. Roy. Soc. London Ser. A* **276**, 238 (1963); **277**, 237 (1963); **281**, 401 (1964).
 - [3] V. I. Anisimov, J. Zaanen, and O. K. Andersen, *Phys. Rev. B* **44**, 943 (1991); V. I. Anisimov, F. Aryasetiawan, and A. I. Lichtenstein, *J. Phys. Cond. Matter* **9**, 767 (1997).
 - [4] W. Metzner and D. Vollhardt, *Phys. Rev. Lett.* **62**, 324 (1989).
 - [5] D. Vollhardt, in *Correlated Electron Systems*, edited by V. J. Emery, World Scientific, Singapore, 1993, p. 57.
 - [6] Th. Pruschke, M. Jarrell, and J. K. Freericks, *Adv. in Phys.* **44**, 187 (1995).
 - [7] A. Georges, G. Kotliar, W. Krauth, and M. J. Rozenberg, *Rev. Mod. Phys.* **68**, 13 (1996).
 - [8] G. Kotliar and D. Vollhardt, *Physics Today* **57**, No. 3 (March), 53 (2004).
 - [9] V. I. Anisimov, A. I. Poteryaev, M. A. Korotin, A. O. Anokhin, and G. Kotliar, *J. Phys. Cond. Matter* **9**, 7359 (1997). The same strategy was formulated by Lichtenstein and Katsnelson, *Phys. Rev. B* **57**, 6884 (1998), as one of their LDA++ approaches.
 - [10] K. Held, I.A. Nekrasov, G. Keller, V. Eyert, N. Blümer, A.K. Mc Mahan, R.T. Scalettar, Th. Pruschke, V.I. Anisimov, and D. Vollhardt, “Realistic investigations of correlated electron systems with LDA+DMFT”, *Psi-k Newsletter* 56 (April 2003), p. 65-103 [psi-k.dl.ac.uk/newsletters/News_56/Highlight_56.pdf].
 - [11] A. I. Lichtenstein, M. I. Katsnelson, G. Kotliar, in *Electron Correlations and Materials Properties*, eds. A. Gonis, N. Kioussis, and M. Ciftan, Kluwer Academic/Plenum, p. 428, New York (2002) [available as cond-mat/0112430].
 - [12] A. Fujimori *et al.*, *Phys. Rev. Lett.* **69**, 1796 (1992).
 - [13] Y. Aiura, F. Iga, Y. Nishihara, H. Ohnuki, H. Kato, *Phys. Rev. B* **47**, 6732 (1993); I.H. Inoue, I. Hase, Y. Aiura, A. Fujimori, Y. Haruyama, T. Maruyama, T. Nishihara, *Phys. Rev. Lett.* **74**, 2539 (1995); I.H. Inoue, O. Goto, H. Makino, N.E. Hussey, M. Ishikawa, *Phys. Rev. B* **58**, 4372 (1998).

- [14] K. Morikawa, T. Mizokawa, K. Kobayashi, A. Fujimori, H. Eisaki, S. Uchida, F. Iga, and Y. Nishihara, Phys. Rev. B **52**, 13711 (1995);
- [15] M. J. Rozenberg, I. H. Inoue, H. Makino, F. Iga, and Y. Nishihara, Phys. Rev. Lett. **76**, 4781 (1996).
- [16] H. Makino, I.H. Inoue, M. J. Rozenberg, I. Hase, Y. Aiura, S. Onari, Phys. Rev. B **58**, 4384 (1998).
- [17] K. Maiti, D.D. Sarma, M. J. Rozenberg, I.H. Inoue, H. Makino, O. Goto, M. Pedio, R. Cimino, Europhys. Lett. **55**, 246 (2001).
- [18] A. Sekiyama, H. Fujiwara, S. Imada, H. Eisaki, S. I. Uchida, K. Takegahara, H. Harima, Y. Saitoh, S. Suga, cond-mat/0206471, superceded by [19].
- [19] A. Sekiyama, H. Fujiwara, S. Imada, S. Suga, H. Eisaki, S. I. Uchida, K. Takegahara, H. Harima, Y. Saitoh, I. A. Nekrasov, G. Keller, D. E. Kondakov, A. V. Kozhevnikov, Th. Pruschke, K. Held, D. Vollhardt, and V. I. Anisimov, Phys. Rev. Lett. **93**, 156402 (2004).
- [20] A. Liebsch Phys. Rev. Lett. **90**, 096401 (2003).
- [21] I. H. Inoue, I. Hase, Y. Aiura, A. Fujimori, K. Morikawa, T. Mizokawa, Y. Haruyama, T. Maruyama and Y. Nishihara, Physica C **235-240**, 1007 (1994).
- [22] I. A. Nekrasov, G. Keller, D. E. Kondakov, A. V. Kozhevnikov, Th. Pruschke, K. Held, D. Vollhardt, and V. I. Anisimov, cond-mat/0211508, superceded by [19].
- [23] E. Pavarini, S. Biermann, A. Poteryaev, A. I. Lichtenstein, A. Georges, O.K. Andersen, Phys. Rev. Lett. **92**, 176403 (2004).
- [24] V. I. Anisimov, D. E. Kondakov, A. V. Kozhevnikov, I. A. Nekrasov, Z. V. Pchelkina, G. Keller, I. Leonov, X. Ren, D. Vollhardt, J. W. Allen, S.-K. Mo, H.-D. Kim, S. Suga, and A. Sekiyama, cond-mat/0407359 [Phys. Rev. B, in press].
- [25] O. K. Andersen and T. Saha-Dasgupta, Phys. Rev. B **62**, R16219 (2000); O. K. Andersen, T. Saha-Dasgupta, S. Ezhov, L. Tsetseris, O. Jepsen, R. W. Tank, C. Arcangeli, and G. Krier, Psi-k Newsletter **45**, 86 (2001); O. K. Andersen, T. Saha-Dasgupta, and S. Ezhov, Bull. Mater. Sci. **26**, 19 (2003).
- [26] I. H. Inoue, private communication.
- [27] M.J. Rey, P.H. Dehault, J.C. Joubert, B. Lambert-Andron, M. Cyrot and F. Cyrot-Lackmann, J. Solid State Chem. **86**, 101 (1990).
- [28] B.L. Chamberland and P.S. Danielson, J. Solid State Chem. **3**, 243 (1971).

- [29] O. K. Andersen, Phys. Rev. B **12**, 3060 (1975); O. Gunnarsson, O. Jepsen, and O. K. Andersen, Phys. Rev. B **27**, 7144 (1983).
- [30] Logarithmic derivatives were fixed to the value $-l - 1$ for Sr(p, f), Ca(p), V(d), O(s, d) states.
- [31] K. Takegahara, J. Electron Spectrosc. Relat. Phenom. **66**, 303 (1995).
- [32] O. Gunnarsson *et al.*, Phys. Rev. B **39**, 1708 (1989).
- [33] I. Solovyev, N. Hamada, and K. Terakura, Phys. Rev. B **53**, 7158 (1996).
- [34] M. B. Zöfl, Th. Pruschke, J. Keller A. I. Poteryaev, I. A. Nekrasov, and V. I. Anisimov, Phys. Rev. B **61**, 12810 (2000).
- [35] J. E. Hirsch and R. M. Fye, Phys. Rev. Lett. **56**, 2521 (1986). For multi-band QMC within DMFT see [10].
- [36] For a review on the maximum entropy method see M. Jarrell and J. E. Gubernatis, Physics Reports **269**, 133 (1996).
- [37] A. Liebsch and A. Lichtenstein, Phys. Rev. Lett. **84**, 1591 (2000).
- [38] I. A. Nekrasov, K. Held, N. Blümer, A. I. Poteryaev, V. I. Anisimov, and D. Vollhardt, Euro. Phys. J. B **18**, 55 (2000).
- [39] K. Held, G. Keller, V. Eyert, V. I. Anisimov, and D. Vollhardt, Phys. Rev. Lett. **86**, 5345 (2001).
- [40] I.A. Nekrasov, Z.V. Pchelkina, G. Keller, Th. Pruschke, K. Held, A. Krimmel, D. Vollhardt, and V.I. Anisimov, Phys. Rev. B **67**, 085111 (2003).
- [41] Ph. Lambin and J. P. Vigneron, Phys. Rev. B **29**, 3430 (1984).
- [42] M. O. Krause and J. H. Oliver, J. Phys. Chem Ref. Data **8**, 329 (1979).
- [43] I. H. Inoue, C. Bergemann, I. Hase, and S. R. Julian, Phys. Rev. Lett. **88**, 236403 (2002).
- [44] It should be noted that the XAS measurements were taken at the Oxygen K-edge. Hence there is no symmetry breaking of the Vanadium 2p shell in the final state. In this case the XAS data can be taken as a good substitute for presently unavailable IPES data.

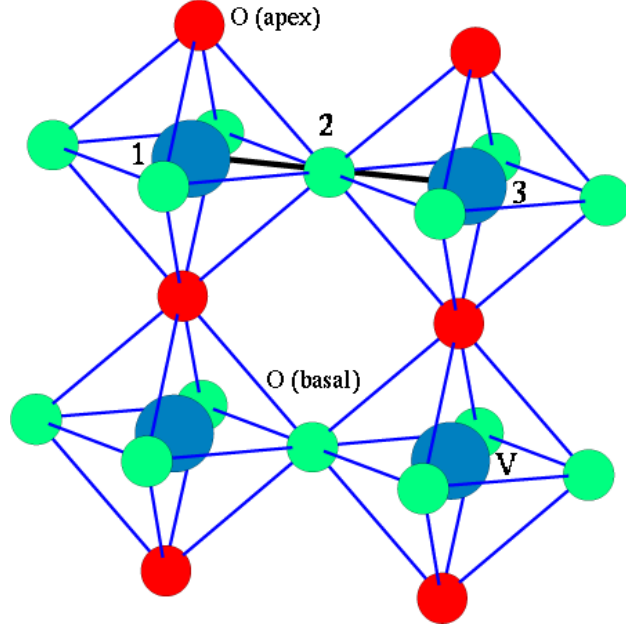


FIG. 1: SrVO_3 , an ideal cubic perovskite, with V-O-V angle $\theta = \angle 123 = 180^\circ$; V: large ions, O_{basal} : small bright ions, O_{apex} : small dark ions.

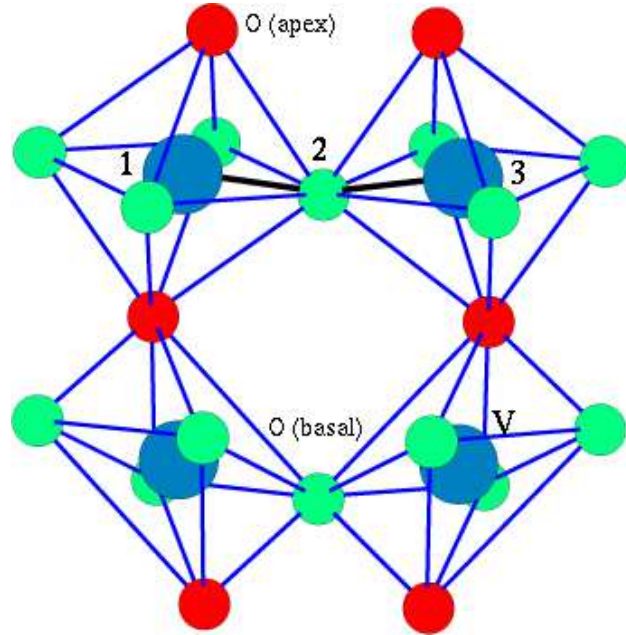


FIG. 2: CaVO_3 , an orthorhombically distorted perovskite, with V-O-V angles $\theta_{\text{basal}} \approx 161^\circ$, $\theta_{\text{plane}} \approx 163^\circ$; V: large ions, O_{basal} : small bright ions, O_{apex} : small dark ions. The local c-axis, later used for the definition of the orbitals, is directed along the tilted V- O_{apex} direction.

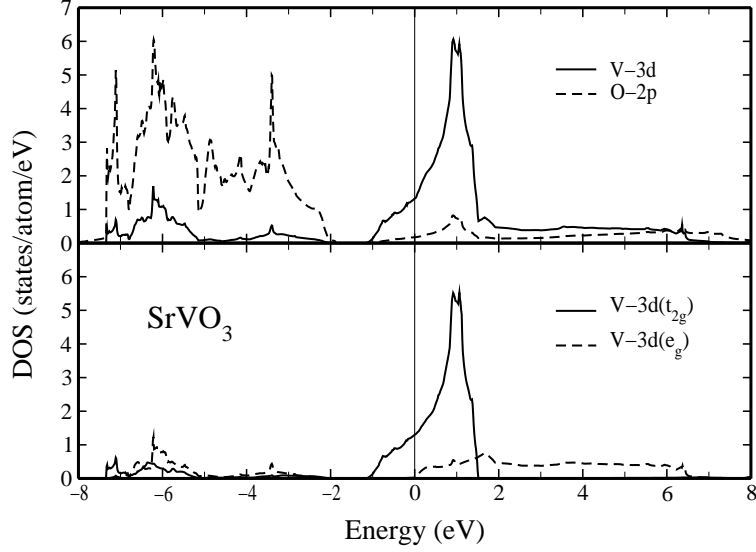


FIG. 3: DOS of SrVO_3 as calculated by LDA(LMTO). Upper panel: V-3d (full line) and O-2p (dashed line) DOS; lower panel: partial DOS of V-3d (t_{2g}) (full line) and V-3d(e_g) (dashed line) orbitals. The Fermi level corresponds to 0 eV.

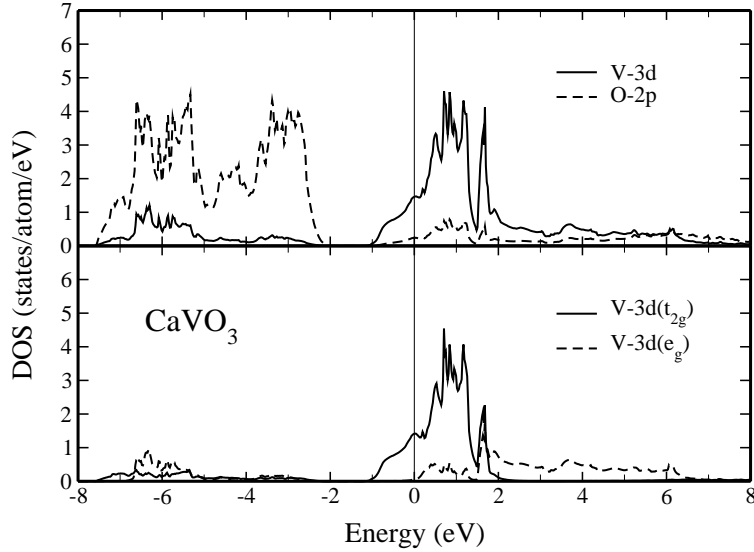


FIG. 4: DOS of CaVO_3 as calculated by LDA(LMTO). Upper panel: V-3d (full line) and O-2p (dashed line) DOS; lower panel: partial DOS of V-3d (t_{2g}) (full line) and V-3d(e_g) (dashed line) orbitals. The Fermi level corresponds to 0 eV.

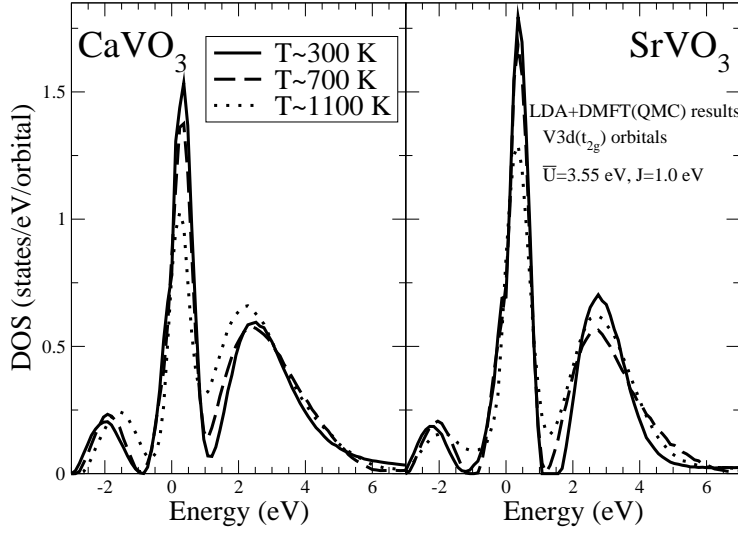


FIG. 5: LDA+DMFT(QMC) spectrum of SrVO_3 (right panel) and CaVO_3 (left panel) calculated at $T \approx 300$ K (solid lines), $T \approx 700$ K (dashed lines), and $T \approx 1100$ K (dotted lines).

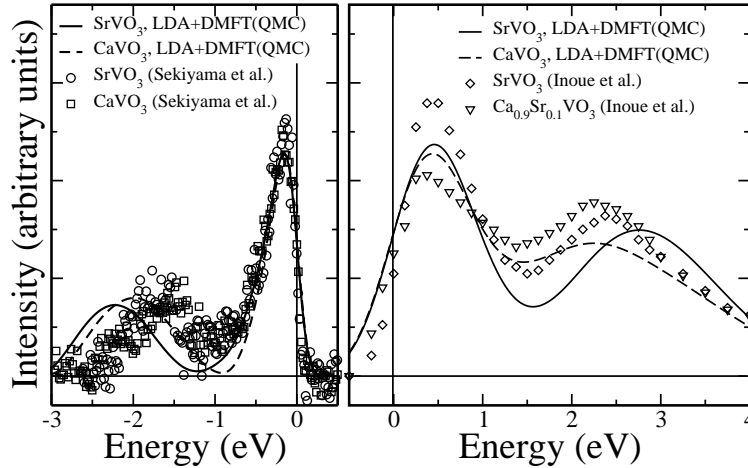


FIG. 6: Comparison of the parameter-free LDA+DMFT(QMC) spectra of SrVO_3 (solid line) and CaVO_3 (dashed line) with experiments below *and* above the Fermi energy. Left panel: high-resolution PES for SrVO_3 (circles) and CaVO_3 (rectangles) [18, 19]. Right panel: 1s XAS for SrVO_3 (diamonds) and $\text{Ca}_{0.9}\text{Sr}_{0.1}\text{VO}_3$ (triangles) [21]. Horizontal line: experimental subtraction of the background intensity.